JOURNAL OF GEOPHYSICAL RESEARCH, VOL. 86, NO. B5, PAGES 3759–3770, MAY 10, 1981

A Study of Regional Temperature and Thermohydrologic Effects of an Underground Repository for Nuclear Wastes in Hard Rock

J. S. Y. WANG, C. F. TSANG, N. G. W. COOK, AND P. A. WITHERSPOON

Earth Sciences Division, Lawrence Berkeley Laboratory, University of California, Berkeley, California 94720

Heat released by the radioactive decay of nuclear wastes in an underground repository causes a long-term thermal disturbance in the rock mass. The nature of this disturbance for a planar repository 3000 m in diameter at a depth of 500 m below surface is investigated. Loaded initially with a power density of 10 W/m^2 of spent fuel assemblies 10 years after discharge from a reactor, the maximum increase in temperature of the repository in granite is about 50°C and the epicentral thermal gradient about 70°C/km. Different waste forms and periods before burial have significant effects on the thermal disturbance. The effects of temperature changes on the groundwater flow are evaluated with simple models of a vertical fracture connected to a horizontal fracture in the rock mass. The buoyancy groundwater flow through the vertical fracture is a function of both the vertical and the horizontal fracture transmissivities, as well as the changes in density and viscosity of groundwater caused by the temperature changes. Finite hydraulic recharge from the surrounding rock mass affects the thermohydrologic disturbance.

INTRODUCTION

Significant quantities of nuclear wastes exist already and continue to be produced [*Department of Energy,* 1978]. At present, most of these wastes are stored in near-surface facilities. Although every precaution is taken to protect man and the environment from the potential hazard posed by these wastes, near-surface storage is not regarded as a satisfactory long-term proposition. Disposal of the nuclear wastes by deep burial in suitable geologic formations is generally favored [*Interagency Review Group on Nuclear Waste Management,* 1978]. The principal attraction of disposal by deep burial is that it provides a high degree of physical isolation of the nuclear waste from the biosphere. The principal concern of deep burial is that at no stage should toxic components of these wastes find their way back to the biosphere at levels which are not completely harmless.

A wealth of scientific knowledge and engineering experience exists concerning the excavation of underground openings in a wide variety of geologic media. Unfortunately, no comparable experience exists concerning the effects of the generation of heat within such openings or of the leakage of materials from such openings back to the biosphere.

Salt formations have generally been preferred as candidates for deep geological disposal for a number of reasons [*National Research Council,* 1957]. The relatively high thermal conduction of salt facilitates the dissipation of heat released by the radioactive decay of nuclear wastes. The viscous plasticity of salt, particularly at elevated temperatures, assures that the excavation within which the wastes are disposed will, in the long term, seal themselves by deformation of the salt itself, and the presence of the salt attests to very slow dissolution and transport by movement of groundwater.

However, other geological media may be equally or even better suited for construction of deep underground repositories for nuclear wastes, provided that the openings and access ways to the repository can be sealed adequately. The permeability of intact pieces of many crystalline and argillaceous rocks is at least as low as that of salt. However, the permeability of masses of such rocks arises mainly from the hydraulic conductivity of joints and fractures pervading them but may still be sufficiently small to retard the movement of groundwater between the repository and the biosphere to an adequate degree.

The purpose of this paper is to study three important aspects concerning the design and performance of such underground repositories for the disposal of nuclear wastes in hard rock. First, the heat released by the radioactive decay of the nuclear wastes causes changes in the spatial and temporal distributions of temperature in the rock mass within which the repository is located. These changes in temperature produce thermally induced components of compressive stress in the heated portions of this rock mass and tensile components of stress outside of this zone. These thermally induced changes in stress may affect the performance and design of a repository. The distribution of temperatures around a repository is necessary to evaluate the thermally induced changes in stress. However, the evaluation of the stress changes is not part of this paper. Second, the magnitude and temporal changes of the temperatures in the rock mass within which the repository is located are affected by the kind of waste and the time after removal from the reactor at which it is buried. The characteristics of different wastes on the temporal changes in temperature are examined. Finally, changes in the temperature of the groundwater in the rock mass containing the repository affect both the density and viscosity of the water significantly. These changes in density and viscosity may result in perturbations of the original hydrologic flow, which could affect the performance of the repository in isolating toxic components of the wastes from the biosphere. A model of buoyancy groundwater flow through a simple fracture system is used to assess the magnitude of this phenomenon.

THERMAL DISTURBANCE

Repository Model

To study the long-term regional changes in temperature in the rock mass, the repository is idealized to be a flat circular disk loaded uniformly with nuclear waste at time $t = 0$. The repository is assumed to be a depth D of 500 m below surface in granite and to have a radius R of 1500 m. The principal mode of heat transfer from the nuclear waste to the rock mass is assumed to be by heat conduction. This has been proved to

Paper number 80B1825.

TABLE 1. Thermal Properties of Rocks

Rock	K, W/m/°C	ρ_R, kg/m^3	C_R, J/kg/°C	κ_T, 10^{-6} m^2/s
Granite*	2.5	2600	836	1.15
Stripa-granite†	3.2	2600	837.36	1.47
Basalt‡	1.62	2865	1164	0.486
Shale§	0.90	2300	1000	0.391

Kappelmeyer and Haenel [1974].
†*Pratt et al.* [1977].
‡*Martinez-Baez and Amick* [1978].
§*Fairchild et al.* [1976].

be a good assumption based on recent Stripa data analysis [*Hood,* 1979].

The temperature field $T(r, z, t)$ resulting from heat conduction in the rock mass is given by a solution to the diffusion equation:

$$\frac{1}{r}\frac{\partial}{\partial r}\left(r\frac{\partial T}{\partial r}\right)+\frac{\partial^2 T}{\partial z^2}=\frac{1}{\kappa_T}\frac{\partial T}{\partial t} \qquad \kappa_T = K/\rho_R C_R \qquad (1)$$

where

- r radial coordinate;
- z vertical coordinate;
- t time after loading;
- κ_T thermal diffusivity;
- K thermal conductivity;
- ρ_R density of the rock;
- C_R specific heat of the rock.

Values for the thermal properties of granite and other hard rocks are given in Table 1.

When heat is released from the nuclear waste at an average rate $\phi(t')$ by the disklike repository from time $t' = 0$ to time $t' = t$, the temperature change at any point (r, z) is

$$\Delta T(r, z, t) = \frac{1}{\rho_R C_R}\int_0^t \phi(t')V_{-D}(r, z, t-t')\,dt' - \frac{1}{\rho_R C_R}\int_0^t \phi(t')V_{+D}(r, z, t-t')\,dt' \qquad (2)$$

The first term in this equation represents the change in temperature from the disklike source in the infinite medium and the second term from an image source is a correction for the presence of a boundary at constant temperature at the ground surface, $z = 0$. The functions $V_{\mp D}$ in (2) are the instantaneous unit-strength disk sources at t' of radius R in the planes $z = \mp D$ [*Carslaw and Jaeger,* 1959]:

$$V_{\mp D}(r, z, t) = \frac{1}{4(\pi\kappa_T{}^3 t^3)^{1/2}} \cdot \int_0^R \exp\left[-\frac{r^2+r'^2+(z\pm D)^2}{4\kappa_T t}\right] I_0\left(\frac{rr'}{2\kappa_T t}\right) r'\,dr' \qquad (3)$$

where I_0 is the zeroth-order modified Bessel function of the first kind.

For the purposes of this paper, (2) and (3) have been solved numerically for a number of expressions $\phi(t')$. Temperatures on the z axis for simple functions of $\phi(t')$, such as constant power, exponential decay of power, and a decrease in power inversely as the square root of time can be expressed in terms of tabulated functions. These are given in Table 2 and can be used to check the accuracy of the numerical solutions to (2) and (3). In this paper, numerical results reproduce these analytical solutions to within 0.01°C.

Different Forms of Waste

At present, consideration is being given to the disposal of two principal forms of nuclear waste generally known as high-level waste. They are spent fuel, as discharged from a reactor, and the products from reprocessing spent fuel to recover the uranium and plutonium. Figure 1 illustrates the power densities of the two principal waste forms from a pressurized water reactor [*Kisner et al.,* 1978]. Either form of high-level waste is assumed to be buried 10 years after discharge from the reactor at an initial loading density of 10 W/m^2 in the plane of the repository. The curves in Figure 1 give, numerically, the values of $\phi(t')$ which are used in (3) to calculate the changes in temperature field. The regional contours of these changes in temperature 100 years and 1000 years after burial are as illustrated in Figures 2 and 3. It is important to note how much greater are the magnitudes of these changes for spent fuel than for reprocessed waste, especially after 1000 years of burial.

TABLE 2. Analytic Solutions of Temperature Rise on the z Axis of Disk Source

Power Form	Power Density $\phi(t)$	Solution Form $f(x, t)$*
Constant	$\phi(0)$	$\frac{\phi(0)(\kappa_T t)^{1/2}}{K}$ ierfc (x)
Exponential decay	$\phi(0)\exp(-\lambda t)$	$\frac{\phi(0)}{K}(\kappa_T/\lambda)^{1/2}$ Im $W[(\lambda t)^{1/2}+ix]$
Inverse square root	$2T_0K/(\pi\kappa_T t)^{1/2}$	T_0 erfc (x)

*$\Delta T(0, z, t) = f\{[(z+D)^2/4\kappa_T t]^{1/2}, t\} - f\{[(R^2+(z+D)^2)/4\kappa_T t]^{1/2}, t\} - f\{[(z-D)^2/4\kappa_T t]^{1/2}, t\} + f\{[(R^2+(z-D)^2)/4\kappa_T t]^{1/2}, t\}$; ierfc, first integral of complementary error function; erfc, complementary error function; Im W, imaginary part of the error function of complex argument.

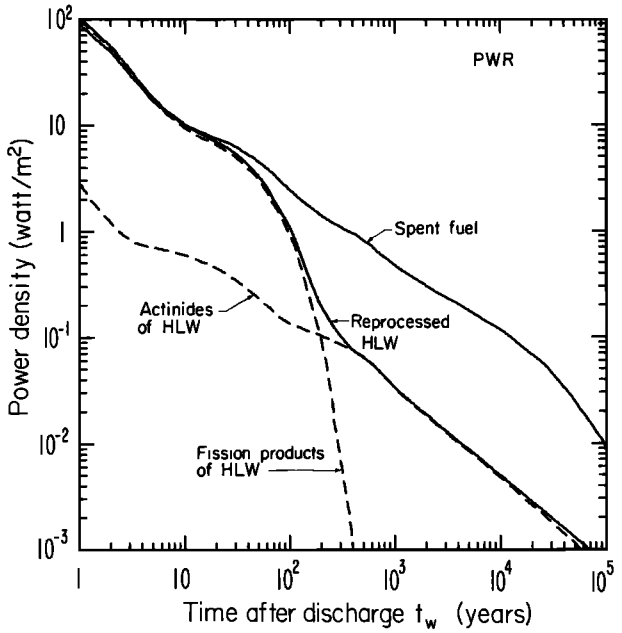

Fig. 1. Areal power density of heat generated by the stored nuclear wastes.

The maximum average temperature in a repository occurs at its center and is plotted as a function of time after burial in Figure 4. For both spent fuel and reprocessed waste this temperature reaches a maximum after a period of less than 100 years and thereafter decays very slowly over a period of many thousands of years. The maximum temperature and all other temperatures are of course proportional to the power density with which the repository is loaded.

To study the far-field effects and, in particular, those at the surface, the maximum ground surface temperature gradient at the epicenter above the repository has been calculated for both forms of waste and is illustrated in Figure 5. This gradient and the corresponding heat flux through the surface reach maximum values at about 2400 years after burial for the spent fuel and 1300 years after burial for the reprocessed waste. The maximum value of the temperature gradient for the spent fuel, 70°C/km, is about 3 times greater than that of the reprocessed waste, 22°C/km. The total thermal gradient is the sum of the original geothermal gradient, typically of 30°C/km, and the thermal gradient induced by the repository.

The decay in power output of nuclear wastes with time is determined by their composition and age. Different fuel cycles yield wastes with different compositions. To evaluate some of these effects, it is assumed that the repository is loaded with 0.01 MTHM/m² (MTHM = metric ton of uranium fuel charged to the reactors). The maximum temperatures and epicentral thermal gradients for different wastes from a pressurized water reactor (PWR) and a boiling water reactor (BWR) are given in Table 3. The same data are illustrated in Figure 6 as a function of time. In Table 3, data are also given for a repository loaded at an initial power density of 10 W/m² for comparison. It can be seen that the differences in temperature for the different fuel cycles arise mainly from variations of initial power loading density. However, significant differences still exist for the results of constant power loading density of 10 W/m².

Near-Surface Cooling Periods

The power output of all nuclear wastes decays very rapidly immediately after discharge from the reactor. Accordingly, the effects of a period of near-surface cooling of these wastes before burial in a repository may be expected to be significant. Table 4 and Figure 7 illustrate the effects on the maximum repository temperatures and epicentral thermal gradients with short periods of near-surface cooling. From these data, it is concluded that the period for which the wastes are cooled near surface before burial is a very important factor in determining the effect of a repository on the temperature of surrounding rock mass.

Repository Depth and Radius

The effects of different repository depths and radii have been analyzed for situations where the ratio of depth to radius is less than 1. The maximum temperature is not significantly

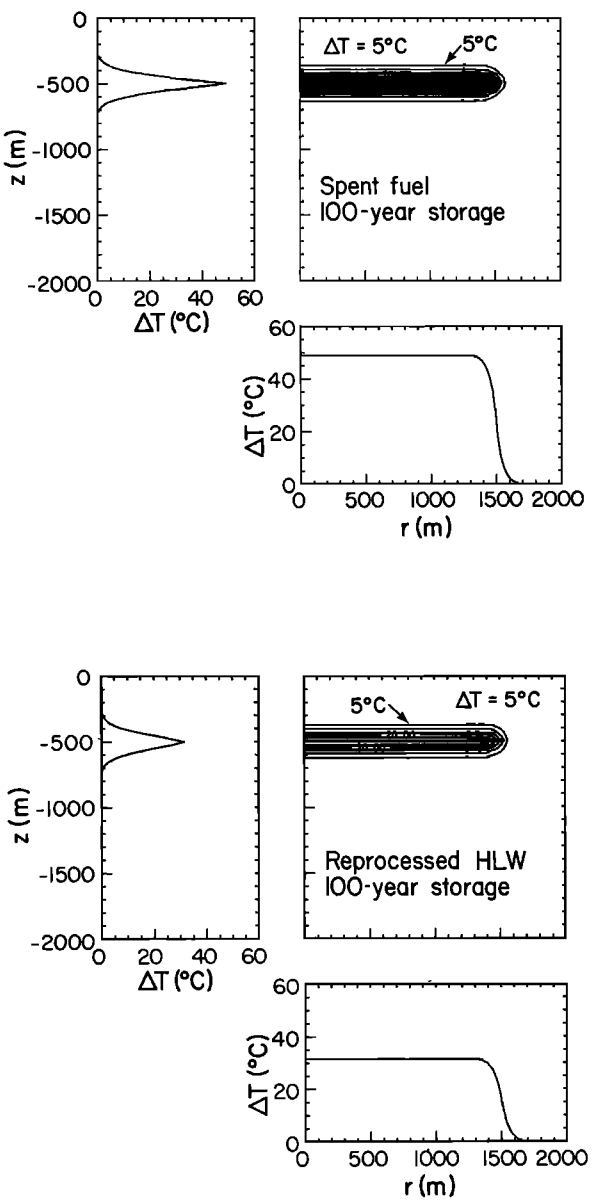

Fig. 2. Isotherms and profiles of temperature rise around repository after 100 years of waste storage.

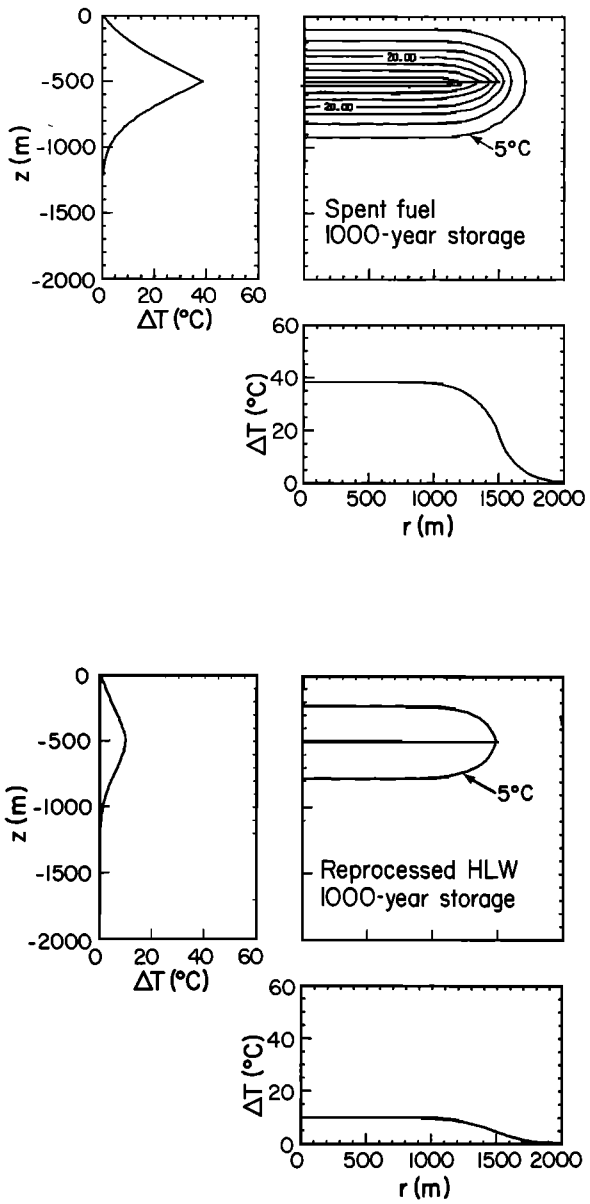

Fig. 3. Isotherms and profiles of temperature rise around repository after 1000 years of waste storage.

affected by this range of depths and radii, but changes in far-field, long-term temperature must be expected. Figure 8 illustrates the dependence of the epicentral thermal gradient with depth and radius.

Rock Properties

The maximum repository temperature and epicentral thermal gradient have been calculated for a repository located within different hard rocks, using the values of thermal properties given in Table 1. From the results illustrated in Figure 9 it can be seen that significant changes in temperature field result from different rock properties.

THERMOHYDROLOGIC DISTURBANCE

Fracture Flow Models

Changes in the temperature of the rock mass containing a repository will change the temperature of the groundwater in this rock mass. Increasing the groundwater temperature results in decreased density and viscosity of the water. In this section the changes in buoyancy groundwater flow induced by these temperature changes are evaluated.

Two types of model geometry are assumed. The first model comprises a simple horizontal fracture at the depth of the repository connecting a recharge zone to a discharge zone and intersecting a vertical fracture containing the axis of the repository as illustrated in Figure 10*a*. Flow from the repository to the surface occurs through the vertical fracture. The effective hydraulic aperture of the horizontal fracture is b_x, and its permeability $k_x = b_x^2/12$ [*Lamb*, 1932; *Snow*, 1965; *Iwai*, 1977; *Witherspoon et al.*, 1980]. The aperture and permeability of the vertical fracture are b_z and $k_z = b_z^2/12$, respectively. The vertical fracture is of distance L_{rc} from the recharge zone and of distance L_{dc} from the discharge zone. For the cases with the width W of the fractures much less than the diameter of the repository, the flows are assumed to be unidirectional along the fractures. The geometry as illustrated in Figure 10*a* will be referred to as the linear flow model. Before the repository is loaded and the rock mass subjected to changes in temperature, it is assumed that the original groundwater flow is horizontal from recharge zone to discharge zone. As the rock mass heats up, so will the groundwater in the vertical fracture containing the center of the repository. This will perturb the original flow pattern.

The second type of geometry studied is that of a radial flow model as illustrated in Figure 10*b*. This corresponds to the first model with the shape of the horizontal fracture changed to be that of a circular disk of radius L. The aperture and permeability of the radial horizontal fracture are b_r and $k_r = b_r^2/12$, respectively. For both models, the flow of groundwater is assumed to be confined within the fractures. In practice, the flow of groundwater through most hard rock, which generally has a very low intrinsic permeability [*Brace et al.*, 1968], is largely through fractures, so that the models approximate the mechanics of groundwater flow through hard rock masses, differing only in their simplicity.

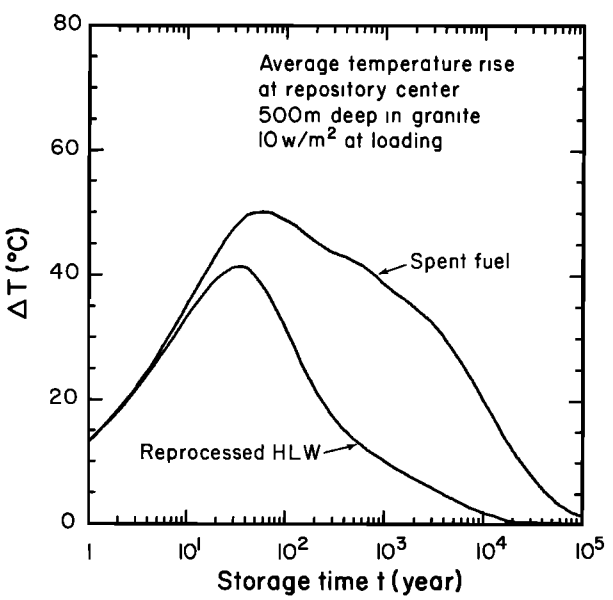

Fig. 4. Temperature rise at the center of a disk-shaped repository in granite stored uniformly with nuclear wastes.

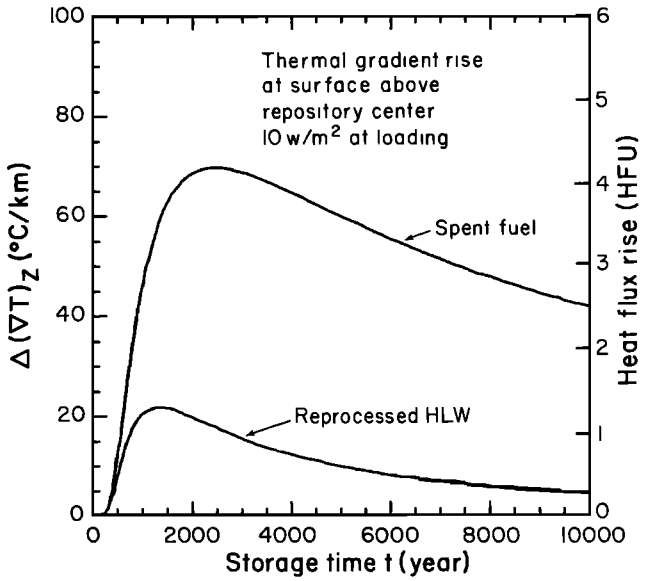

Fig. 5. Ground surface epicentral thermal gradient rise above a disk-shaped nuclear waste repository with radius of 1500 m and 500 m deep in granite.

Flow Equations

For any temperature field the flow of the groundwater must satisfy the equations of conservation of mass and momentum. The equation for the conservation of mass is

$$\frac{\partial \rho}{\partial t} + \nabla \cdot \mathbf{q} = 0 \tag{4}$$

where $\mathbf{q}$ is the mass flux that is the product of the density and velocity of the water in the fracture, ρ is density of water, and t is time.

In most studies of thermal convection, because of the small compressibility of water, it is usual to make use of the Boussinesq approximation [*Wooding*, 1957; *Combarnous and Bories*, 1975] that variations in the density of water with time can be neglected except for the effects on the buoyancy of the groundwater. As a result of this, (4) reduces to

$$\nabla \cdot \mathbf{q} = 0 \tag{5}$$

For low velocities, inertial forces are much less than viscous forces, so that by means of Darcy's law the equation of momentum can be written as:

$$\nabla P + \frac{\nu}{k}\mathbf{q} - \rho \mathbf{g} = 0 \tag{6}$$

where

P pressure;
ν kinematic viscosity of water;
k permeability;
$\mathbf{g}$ gravitational acceleration.

Equations (5) and (6) describe the incompressible flow of groundwater.

The first case considered is the linear flow model with zero original groundwater flow and with the repository located midway between the recharge and discharge zones, $L_{rc} = L_{dc} = L$. The flow is symmetric about $x = 0$ with boundary conditions

$$P(t) = 0 \quad \text{at} \quad x = 0 \quad z = 0 \tag{7}$$

$$b_x q_x(t) + \tfrac{1}{2} b_z q_z(t) = 0 \quad \text{at} \quad x = 0 \quad z = -D \tag{8}$$

$$P(t) = P_0 = \int_{-D}^{0} \rho_0(z) g \, dz \quad \text{at} \quad x = L \quad z = -D \tag{9}$$

The water table is assumed to be at the surface $z = 0$ with zero hydraulic pressure in (7). Equation (8) describes Kirchoff's law for the junction between vertical and horizontal fractures. P_0 in (9) is the hydrostatic pressure imposed at the inlet of the horizontal fracture.

In accordance with (5), the unidirectional flows are inde-

TABLE 3. Effects of Fuel Cycles

Fuel Cycle*	$(\Delta T)_{max}$,† °C	$(\Delta(\nabla T)_z)_{max}$,† °C/km	Power Density at Loading W/m²	Power Density at Loading kW/Canister
	Nuclear Reactor PWR			
Spent fuel	60 (50)	83 (70)	11.9 (10)	0.548
HLW + PuO_2: U recycle	65 (52)	86 (69)	12.5 (10)	2.61
HLW: U + Pu recycle	90 (40)	68 (30)	22.7 (10)	4.75
HLW: U recycle	43 (42)	22 (22)	10.2 (10)	2.14
HLW: no recycle	43 (41)	22 (22)	10.3 (10)	2.16
	Nuclear Reactor BWR			
Spent fuel	50 (51)	73 (74)	9.96 (10)	0.182
HLW + PuO_2: U recycle	57 (54)	77 (73)	10.5 (10)	2.20
HLW: U + Pu recycle	71 (40)	59 (34)	17.5 (10)	3.65
HLW: U recycle	35 (42)	19 (23)	8.30 (10)	1.74
HLW: no recycle	35 (42)	19 (23)	8.35 (10)	1.75

Values without parentheses correspond to 0.01-MTHM/m² waste capacity. Values with parentheses correspond to 10-W/m² power density.

*Spent fuel—fuel assembly discharge directly from the reactor. HLW + PuO_2: U recycle—reprocessed waste with U and Pu removed from the discharge fuel, U recycled in the reactor, and Pu stored together with the water. HLW: U + Pu recycle—reprocessed waste with U and Pu removed from the discharge fuel and recycled in the mixed oxide reactor. HLW: U recycle—reprocessed waste with U and Pu removed from the discharge fuel and U recycled in the reactor. HLW: no recycle—reprocessed waste with U and Pu removed from the discharge fuel.

†$(\Delta T)_{max}$: maximum value of the average temperature rise at the center of repository. $(\Delta(\nabla T)_z)_{max}$: maximum value of the ground surface thermal gradient rise at the epicenter above the repository.

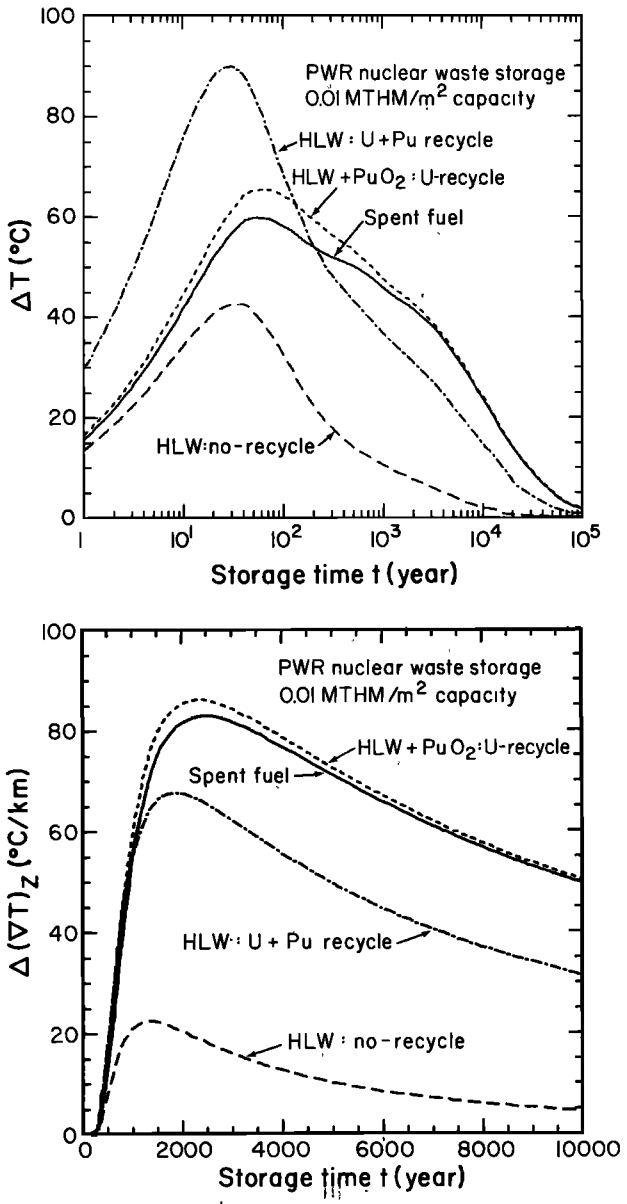

Fig. 6. Effects of different PWR fuel cycles from the same amount of fuel on the repository temperature and ground surface thermal gradient.

pendent of the spatial coordinates along the fractures. With constant flow, (6) can be integrated from the repository center to the boundaries:

$$0 - P(0, -D, t) = -\frac{q_z(t)}{k_z}\int_{-D}^{0} \nu(0, z, t)\, dz - \int_{-D}^{0} \rho(0, z, t)\, g\, dz \tag{10}$$

$$P_0 - P(0, -D, t) = -\frac{q_x(t)}{k_x}\int_{0}^{L} \nu(x, -D, t)\, dx \tag{11}$$

Equations (8), (10), (11) can be solved for the unknowns $q_z(t)$, $q_x(t)$, and $P(0, -D, t)$. The result for $q_z(t)$ is

$$q_z(t) = \frac{k_z \rho_0 g}{\nu_0} \cdot \frac{i_B}{1 + Fb_z k_z / b_x k_x} \tag{12}$$

where

- $k_z\rho_0 g/\nu_0$ hydraulic conductivity of the vertical fracture with constant density and viscosity at surface temperature;
- i_B buoyancy hydraulic gradient;
- F recharge retardation parameter;
- $b_z k_z$ vertical transmissivity (aperture-permeability product of vertical fracture);
- $b_x k_x$ horizontal transmissivity (aperture-permeability product of horizontal fracture).

The buoyancy hydraulic gradient i_B depends only on the vertical variations of density and viscosity:

$$i_B(t) = \frac{\langle \Delta\rho g D \rangle}{\rho_0 g D} \cdot \frac{\nu_0}{\bar{\nu}_z} \tag{13}$$

where $\bar{\nu}_z$ is the averaged viscosity over the flow path along the vertical fracture from $z = -D$ to $z = 0$ and $\langle \Delta\rho g D \rangle$ is the buoyancy-driving pressure

$$\langle \Delta\rho g D \rangle = \int_{-D}^{0} [\rho_0(z) - \rho(0, z, t)] g\, dz \tag{14}$$

The density $\rho(0, z, t)$ in (14) is calculated at temperature $T_0(z) + \Delta T(0, z, t)$, and $\rho_0(z)$ at $T_0(z)$. The ambient temperature may be given by $T_0(z) = (20 - 0.03z)$°C with a surface temperature of 20°C and an original geothermal gradient of 30°C/km.

TABLE 4. Effects of Surface Cooling

Surface Cooling Period, years	$(\Delta T)_{max}$,* °C	$(\Delta(\nabla T)_z)_{max}$,*°C/km	Power Density at Loading W/m²	Power Density at Loading kW/Canister
		Spent Fuel of PWR		
1	98 (9)	93 (9)	104. (10)	4.81
2	76 (14)	90 (16)	56.4 (10)	2.60
5	67 (33)	86 (43)	20.1 (10)	0.927
10	60 (50)	83 (70)	11.9 (10)	0.548
		Reprocessed HLW: No Recycle of PWR		
1	95 (9)	35 (3)	103. (10)	21.5
2	62 (11)	31 (6)	55.0 (10)	11.5
5	50 (27)	26 (14)	18.7 (10)	3.9
10	43 (41)	22 (22)	10.3 (10)	2.16

Values without parentheses correspond to 0.01-MTHM/m² waste capacity. Values with parentheses correspond to 10-W/m² power density.

*$(\Delta T)_{max}$: maximum value of the average temperature rise at the center of repository. $(\Delta(\nabla T)_z)_{max}$: maximum value of the ground surface thermal gradient rise at the epicenter above the repository.

†Values without parentheses correspond to 0.01-MTHM/m² waste capacity. Values with parentheses correspond to 10-W/m² power density.

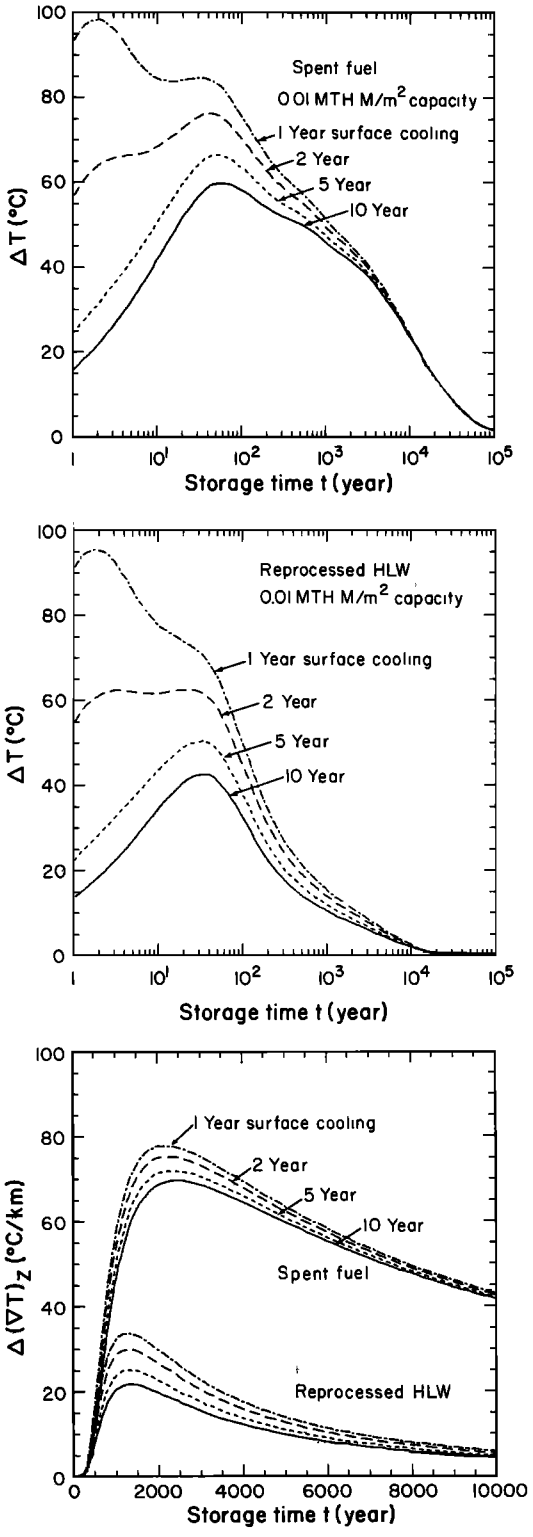

Fig. 7. Effects of surface cooling periods of wastes with density of 0.01 MTHM/m² on the repository temperature and ground surface thermal gradient.

The recharge retardation parameter in (12) is

$$F(t) = \frac{L}{2D} \cdot \frac{\bar{\nu}_x}{\bar{\nu}_z} \tag{15}$$

The geometric factor in F is the ratio $L/2D$; $\bar{\nu}_x$ is the average of viscosity over the flow path along the horizontal fracture from $x = 0$ to $x = L$.

Equation (12) for $q_z(t)$ can be generalized to the cases with nonzero original groundwater flow and with nonequal distances from the repository to the recharge and discharge zones, $L_{rc} \neq L_{dc}$. By solving the whole flow system with the vertical and both horizontal flow paths in Figure 10*a* and with the water table head equal to h_{rc} at the recharge zone and equal to h_{dc} at the discharge zone, the expression for $q_z(t)$ is

$$q_z(t) = \frac{k_z \rho_0 g}{\nu_0} \cdot \frac{i_B + i_0 \nu_0 (\bar{\nu}_{rc}^{-1} - \bar{\nu}_{dc}^{-1})[(L_{rc}\bar{\nu}_{rc})^{-1} + (L_{dc}\bar{\nu}_{dc})^{-1}]^{-1}(D\bar{\nu}_z)^{-1}}{1 + [(L_{rc}\bar{\nu}_{rc})^{-1} + (L_{dc}\bar{\nu}_{dc})^{-1}]^{-1}(D\bar{\nu}_z)^{-1}(b_z k_z / b_x k_x)} \tag{16}$$

Equation (16) is similar to (12) with minor modification in the driving gradient by the original hydraulic gradient $i_0 = (h_{rc} - h_{dc})/(L_{rc} + L_{dc})$. The denominator of (16) is of the same form of (12), but the slight difference between the averages of viscosity over the recharge and discharge flow paths, $\bar{\nu}_{rc}$ and $\bar{\nu}_{dc}$,

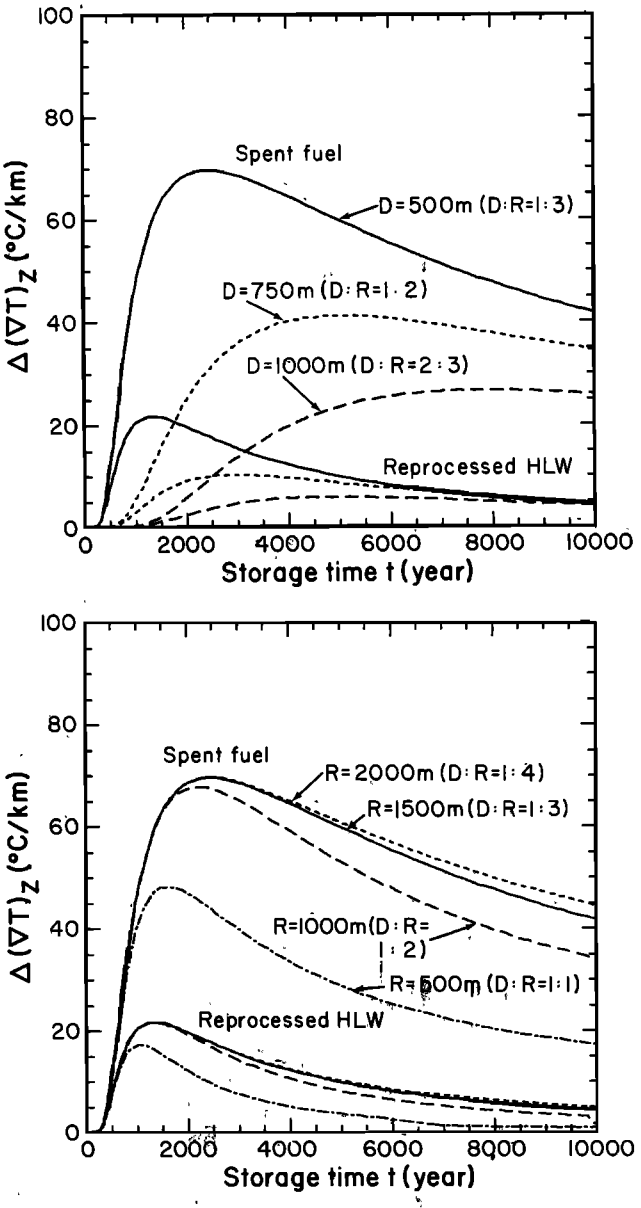

Fig. 8. Effects of different depths and radii of repository on the ground surface thermal gradient.

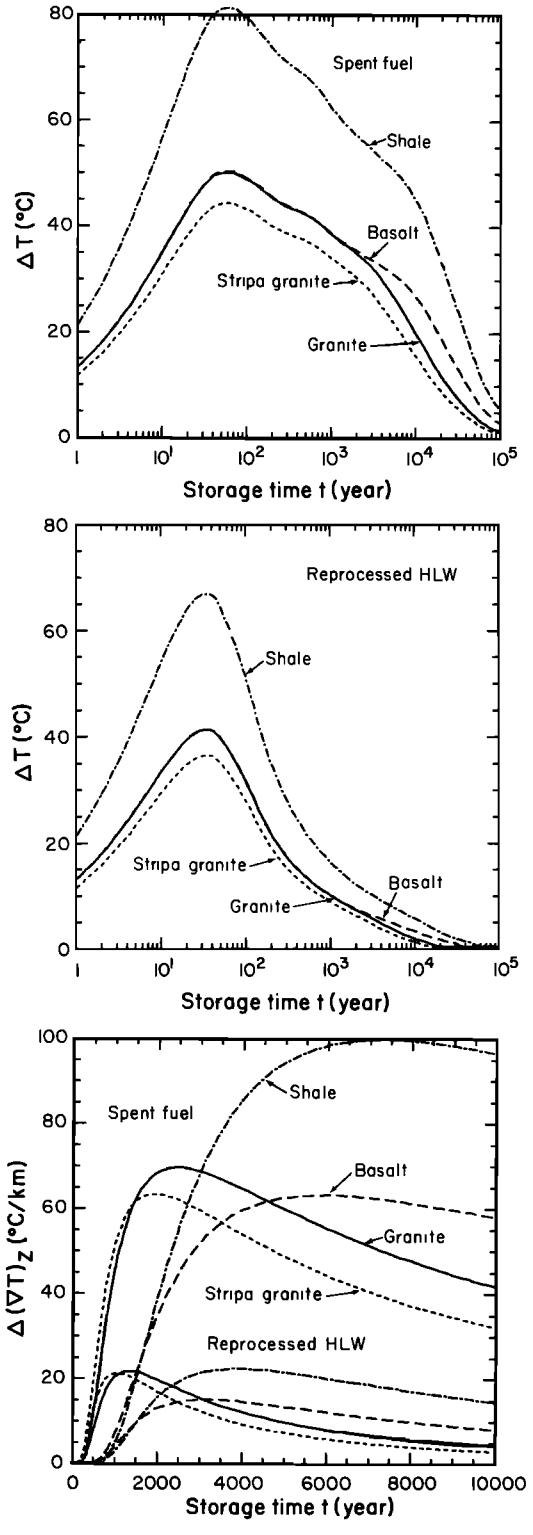

Fig. 9. Effects of rock formations on the repository temperature and ground surface thermal gradient.

has been taken into account in the recharge retardation parameter.

For the radial flow model with horizontal fracture extended beyond the repository to surrounding recharge zone as illustrated in Figure 10*b*, the recharge to buoyancy flow comes from all directions. The vertical fracture in the radial flow model is the same as that in the linear flow model with upward flow from the repository to the surface. However, it is assumed that the horizontal flow is radial for $r \geq R$. With radial symmetry, the product rq_r is constant in accordance with (5). The Darcy equation (6) can be integrated from $r = R$ to $r = L$ to obtain the pressure difference between the repository and the outer boundary. Within the repository the pressure drop from the rim of the repository to the inlet of the vertical fracture is neglected. This assumption is justified if the permeability of the back-filled material for the repository is much higher than the permeability of the surrounding fracture. In the linear flow model, the flow path from $x = 0$ to $x = R$ is treated as part of the horizontal fracture. This portion of the flow path can be neglected if the same assumption about the permeability in the repository is made.

With the modifications to radial geometry, Kirchoff's law for the connection between the vertical fracture and the radial fracture is

$$2\pi R b_r q_r(R, t) + W b_z q_z(t) = 0 \tag{17}$$

Other boundary conditions and solution procedures are similar to those in the linear flow model. The result for the vertical buoyancy flow $q_z(t)$ is nearly identical with (12) of the linear flow model:

$$q_z(t) = \frac{k_z \rho_0 g}{\nu_0} \cdot \frac{i_B}{1 + F b_z k_z / b_r k_r} \tag{18}$$

with radial transimissivity replacing the linear horizontal transmissivity. The recharge retardation parameter is different:

$$F(t) = \frac{W \ln (L/R)}{2\pi D} \cdot \frac{\bar{\nu}_r}{\bar{\nu}_z} \tag{19}$$

The main difference between (19) of the radial flow model and (15) of the linear flow model is the geometric ratio factor; $\bar{\nu}_r$ in (19) is the average of viscosity, weighted by r^{-1}, over the radial flow region from $r = R$ to $r = L$.

Buoyancy Flow

The vertical buoyancy flow $q_z(t)$ in (12), (16), or (18) depends on the buoyancy hydraulic gradient, the vertical hydraulic conductivity, the recharge retardation parameter, and ratio of the vertical and horizontal hydraulic transmissivities.

Consider first the case of a linear flow model with equal apertures for the vertical and horizontal fractures, $b_z = b_x = 1$ μm, and with equal distances to the recharge and discharge zones, $L_{rc} = L_{dc} = 5000$ m. The vertical buoyancy flow can be evaluated by numerical integration of the buoyancy driving pressure along the vertical flow path and the averages of viscosity along the vertical and horizontal flow paths. To calculate the displacement of water in the vertical fracture, $q_z(t)$ can be integrated over time. The groundwater initially at the depth of the repository will move upward in the vertical fracture as a function of time after burial of the wastes. The results of one repository at depth of 500 m are illustrated in Figure 11. For comparison, the results of another repository at depth 1000 m are also included.

The vertical flow in the case of spent fuel is substantially greater than that of reprocessed waste. The buoyancy movement of groundwater is proportional to the change in temperature of the rock mass, and the temperature disturbance induced by a spent fuel repository is significantly higher than

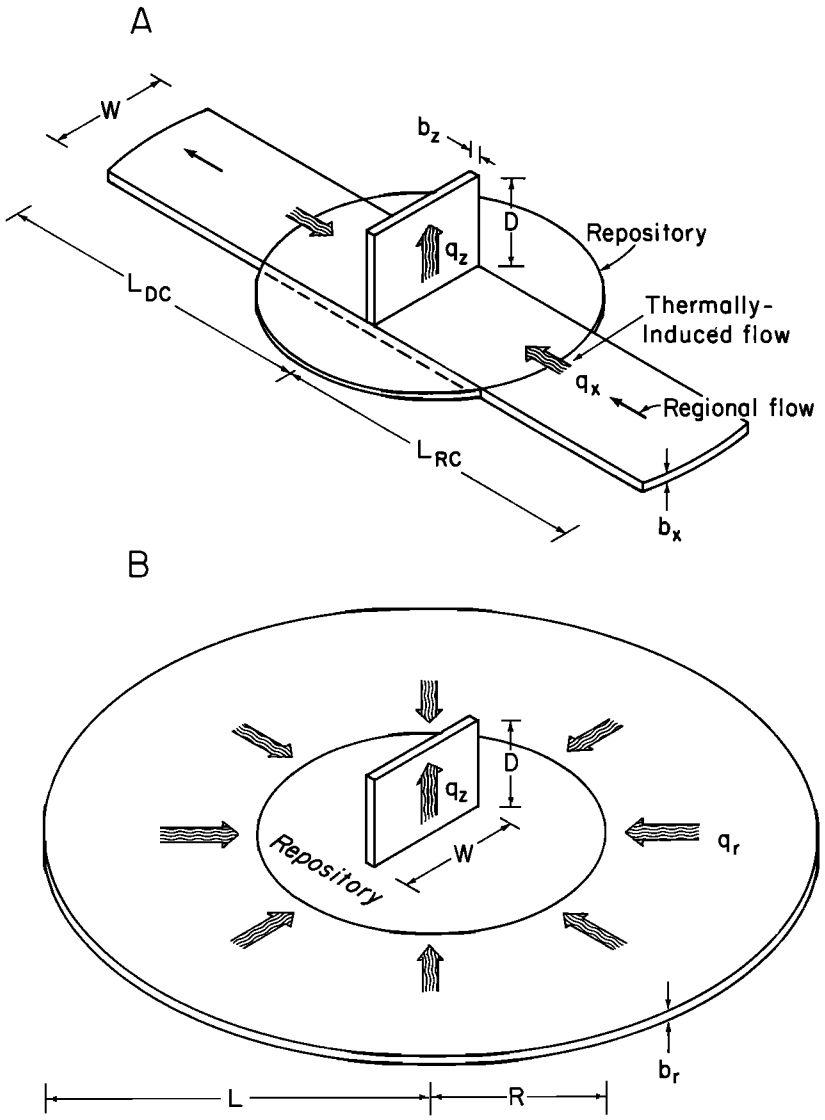

Fig. 10. Two-fracture models for simulating buoyancy groundwater movement through a repository: (*a*) linear flow model and (*b*) radial flow model.

that by a reprocessed waste repository (see Figure 3). On the other hand, there is little difference for the cases with different depths. Thus it appears that the flow of water in the vertical fracture depends upon the integral of the buoyancy force throughout the length of the vertical fracture, which is a function mainly of the total heat released from the repository.

The main driving force for the buoyancy flow is due to the contrast in density between the heated water near the repository with temperature $T_0 + \Delta T$ and the ambient water in the recharge and discharge zones with temperature T_0. Figure 12 illustrates the weak dependence of buoyancy flow on the natural geothermal gradient. The slight differences for different geothermal gradients result mainly from the temperature dependence of viscosity. The general formulae [*Meyer et al.*, 1967] of density and viscosity of water as nonlinear functions of temperature and pressure are used in our calculations.

Recharge Resistance

In addition to the buoyancy of the heated water in the vertical fracture, the flow of this water is affected by the hydrologic connections and conditions. The horizontal fracture represents the recharge flow path. The shorter the distance L from repository to recharge zone, the less the recharge resistance, and the greater the flow of water in the vertical fracture for a given buoyancy. As examples, the velocity $v_z(t) = q_z(t)/\rho_0$ for $L = 0$, 2000, 5000, and 10,000 m is plotted in Figure 13. The buoyancy flow is proportional to an effective vertical gradient:

$$i_z(t) = \frac{i_B}{1 + Fb_z k_z / b_x k_x} \tag{20}$$

where the recharge retardation factor $F \simeq 0.5\ L/D$ for the linear flow model (see (15)). The results of v_z and i_z for the linear flow model in Figure 13 illustrate the sensitive dependence of buoyancy flow on the magnitude of F. From the figure it is apparent that the curves for a 500-m and a 1000-m-deep repository have approximately the same maximum values of the buoyancy velocity when they have the same L/D ratio or F value.

Although the case with $L = 0$, or equivalently $F = 0$, has a

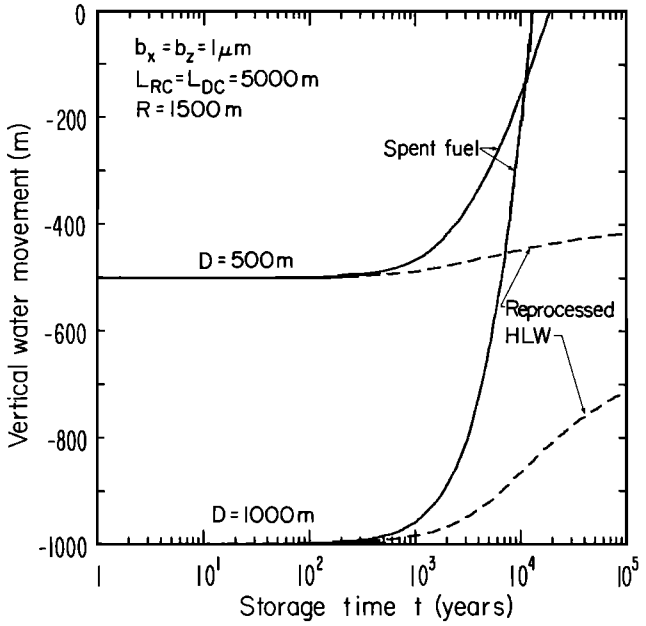

Fig. 11. Water movement along vertical fracture from the repository (linear flow model).

large buoyancy flow, it is an unrealistic representation of the hydrologic condition of a repository. The geometry of $L = 0$ in the linear flow model represents a situation where instant recharge is available to the vertical fracture flow at its inlet end near the center of the repository. For a low-permeability formation suitable for a repository, the recharge zones should be some distance away from the repository.

In general, $F \neq 0$, and the effective vertical gradient i_z in (20) depends on the ratio of the vertical and horizontal fracture transmissivities. The buoyancy flow is no longer simply proportional to the vertical permeability k_z or b_z^2. Except for

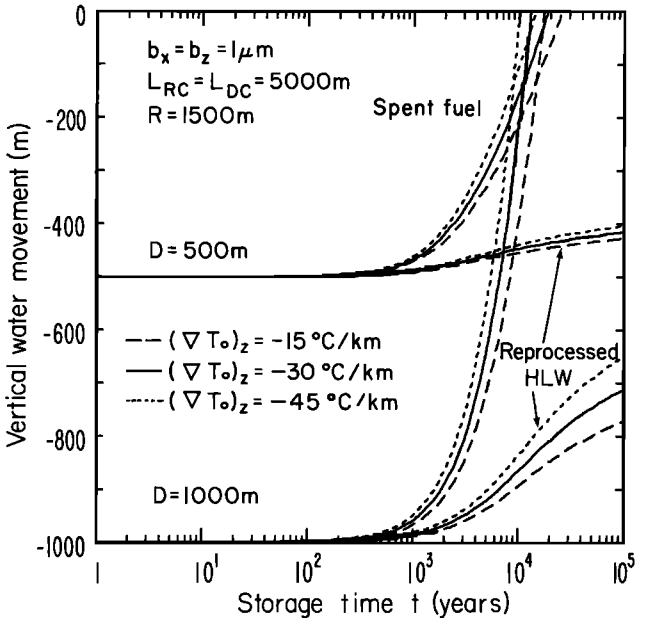

Fig. 12. Effects of different original geothermal gradients on the water movement along the vertical fracture from the repository (linear flow model).

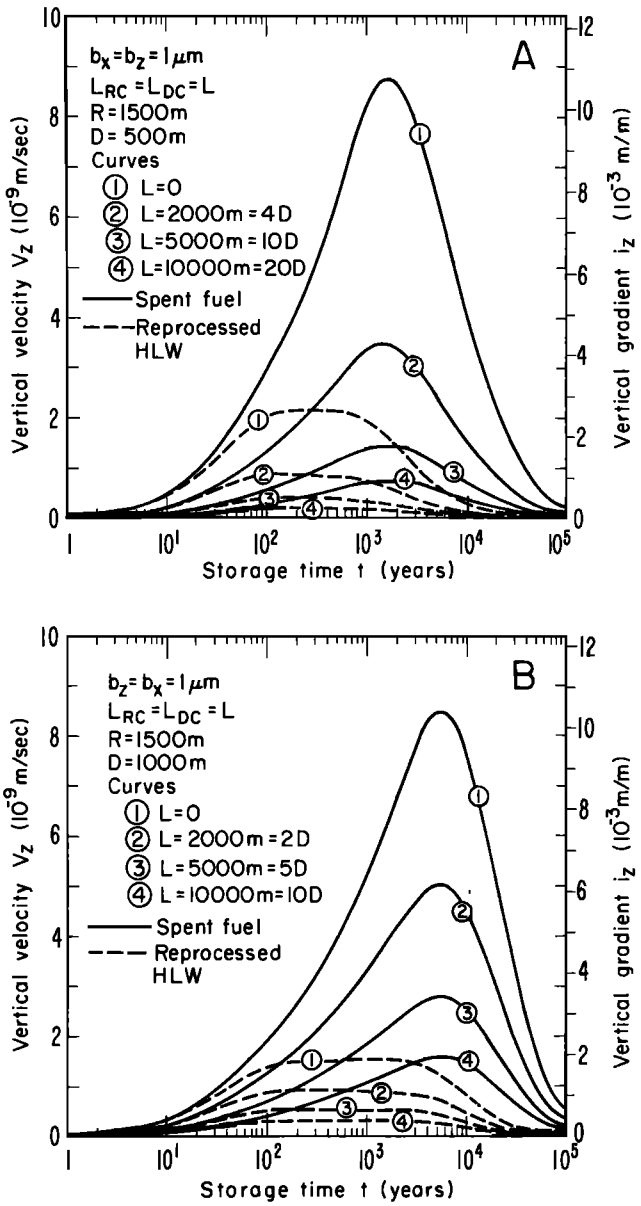

Fig. 13. Effects of recharge distances L on the flow velocities and hydraulic gradients along the vertical fracture from (*a*) 500-m-deep and (*b*) 1000-m-deep repository (linear flow model).

the condition that the resistance factor $Fb_zk_z/b_xk_x \ll 1$, $q_z(t)$ does not increase as b_z increases. On the contrary, the buoyancy flow $q_z(t)$ approaches zero as b_z increases to infinity. The b_z^3 dependance in the resistance factor overcomes the b_z^2 dependence in the permeability. With a limited recharge (b_x, k_x constant), the buoyancy gradient cannot effectively drive the large amount of water in a large vertical fracture. It can be shown that at a given time, $q_z(t)$ is maximum with $b_z = (2/F)^{1/2}b_x$ and

$$q_z(t) < \frac{1}{3}\frac{k_x\rho_0 g}{\nu_0}\left[\frac{2}{F}\right]^{2/3} i_B \qquad (21)$$

Thus buoyancy groundwater flow in the vertical fracture is limited by the permeability of the horizontal fracture rather than the permeability of the vertical fracture. In Figure 14, results with a constant aperture $b_x = 1$ μm and with a range of

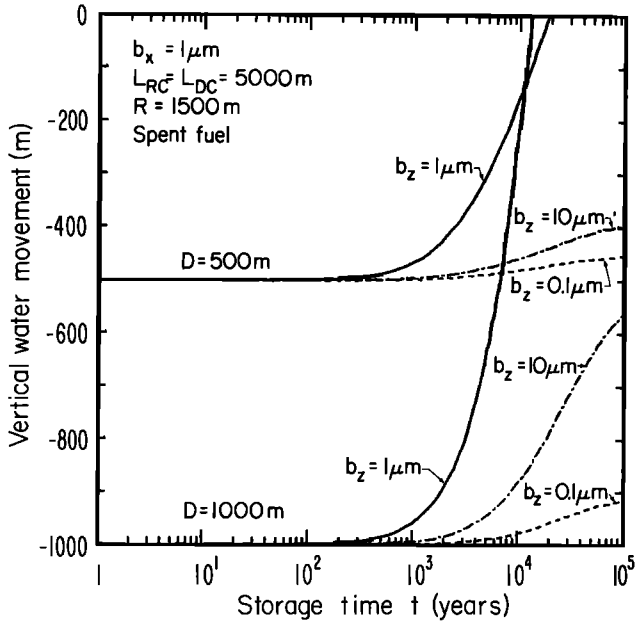

Fig. 14. Effects of different vertical fracture apertures on the water movement along the vertical fracture from the repository (linear flow model).

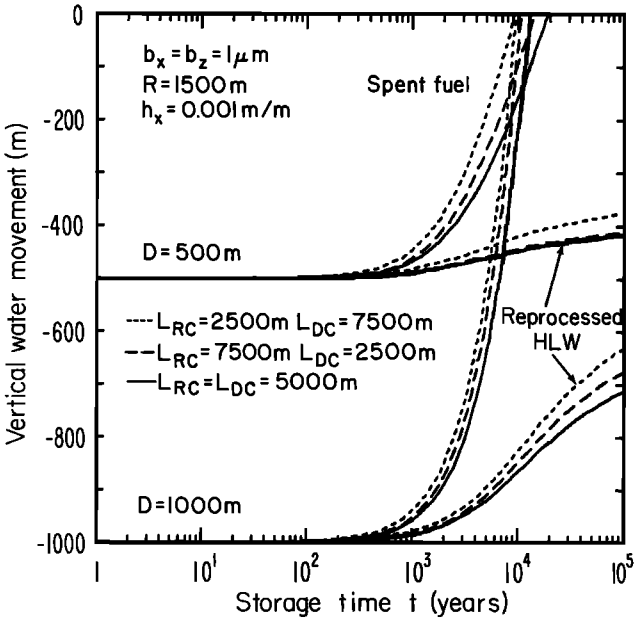

Fig. 15. Effects of different recharge distance L_{rc} and discharge distance L_{dc} on the water movement along the vertical fracture from the repository (linear flow model).

apertures b_z = 10, 1, and 0.1 μm are illustrated. The movement of the groundwater in the vertical fracture is significantly slower both for the case of $b_z = 10b_x$ and $b_z = 0.1b_x$ than with $b_z = b_x$.

All the preceding results have been calculated for the symmetric repository location. In Figure 15 the effects of the position of the repository between the recharge and discharge zones are illustrated. The original hydraulic gradient i_0 is assumed to be 0.001 m/m in the calculation of $q_z(t)$ in (16). The results indicate that the coupling between the buoyancy flow and the original groundwater flow is small in this model. It should be noted that (16) reduces to (12) for $L_{rc} = L_{dc}$ even when $i_0 \neq 0$. In other words, for the symmetric case, the buoyancy flow in the vertical fracture is independent of the original groundwater flow in the horizontal direction.

Consider next the radial flow model which represents a different recharge geometry. The recharge retardation factor in (19) is $F \simeq W \ln (L/R)/2\pi D$. In comparison with the linear case, the radial model with recharge from all directions is less sensitive to the distance L from the repository to the outer boundary. The hydrologic parameters of recharge distance L = 5000 m, vertical fracture width W = 2000 m, and repository radius R = 1500 m are used in the calculations, and the results are shown in Figures 16 and 17. The buoyancy flow is faster in the radial model than the corresponding result of L = 5000 m in the linear model in Figures 13 and 14. However, the qualitative dependences of buoyancy flow on the transmissivity ratio and on the depth of the repository are the same for both models.

Under the condition that the buoyancy flow is limited by the recharge, either because of long recharge distances or small horizontal-vertical transmissivity ratio, the resistance factor Fb_zk_z/b_xk_x or Fb_zk_z/b_rk_r will be much greater than 1. In this case, $q_z(t)$ is proportional to F^{-1} or to the depth D for both models (see (15) and (19)). Hence the time required for the water movement from depth to the surface, which is roughly proportional to D/q_z, is insensitive to the change in depth.

DISCUSSION

Although the thermohydrologoic model used for the analysis presented in this paper is very simple, it should possess the same physical behavior as that of the more complex systems of fractures which account for the permeability of masses of hard rock. Accordingly, it should provide a good insight into the dynamics of thermally-induced groundwater flow, and illustrate the sensitivity of this flow to various parameters. However, the actual numerical results should be considered as no more than order of magnitude estimates. It must be pointed out also that the transport of nuclides from the reposi-

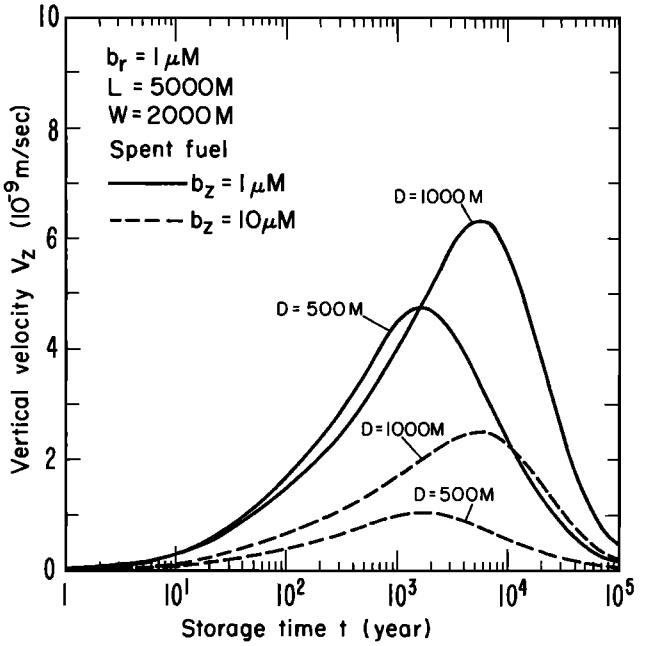

Fig. 16. Flow velocities along vertical fracture with different vertical fracture apertures and depths for L = 5000 m (radial flow model).

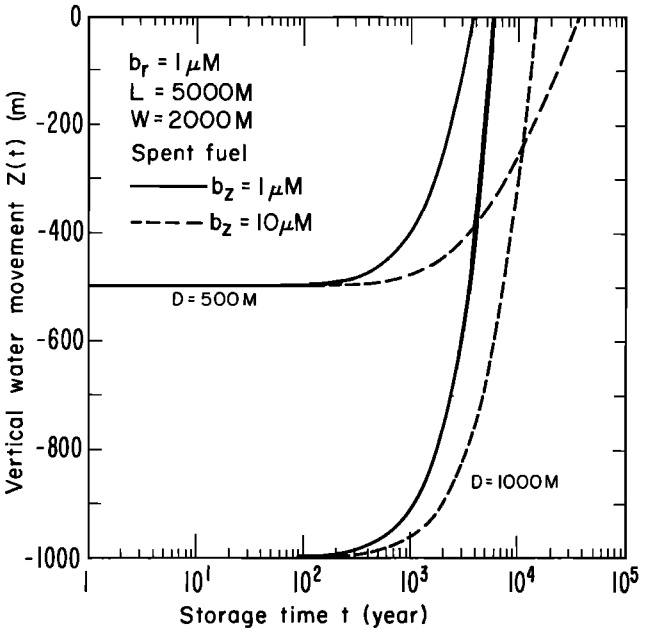

Fig. 17. Water movement along vertical fracture from the repository (radial flow model).

tory to surface does not take place at the same rate as that of the groundwater. Nuclide transport is retarded in a certain degree as the result of physical and chemical processes, such as sorption.

The calculations reported in this paper suggest that under certain circumstances, thermally induced buoyancy groundwater flow may be a mechanism by which toxic materials from a repository could be transported to the biosphere. The magnitude of this flow depends upon many factors. Of these, the aggregate increase in the temperature of the rock mass containing the repository is one of the most important. This temperature is affected by the design of the repository, the kind of nuclear waste buried in it, and the period for which this waste has been cooled near surface before burial. Significant differences exist between reprocessed waste and spent fuel in respect of the degree to which the rock mass is heated and hence the time taken for groundwater to reach the surface by buoyancy flow. The depth of the repository below surface is of much less significance. Cooling of the wastes near surface can be used to compensate for these differences and reduce substantially the total amount of heat put into the rock mass. The thermal conductivity of different kinds of rocks has significant effect on thermally induced disturbance too. Finally, the buoyancy groundwater flow depends upon the ratio of the hydraulic transmissivities of the vertical and horizontal fractures, the maximum flow being determined by the transmissivity of the horizontal fracture.

Acknowledgment. This work is supported by the U.S. Department of Energy under contract W-7405-ENG-48.

REFERENCES

Brace, W. F., J. B. Walsh, and W. T. Frangos, Permeability of granite under high pressure, *J. Geophys. Res., 73*(6), 2225–2236, 1968.

Carslaw, H. S., and J. C. Jaeger, *Conduction of Heat in Solids,* 2nd ed., p. 260, Oxford at the Clarendon Press, London, 1959.

Combarnous, M. A., and S. A. Bories, Hydrothermal convection in saturated porous media, *Advan. Hydrosci., 10,* 231–307, 1975.

Department of Energy, Report of task force for review of nuclear waste management, *Rep. DOE/ER-0004/D,* Washington, D. C., Feb. 1978.

Fairchild, P. D., G. D. Brunton, and J. F. Cuderman, National waste terminal storage program on radioactive waste storage, *progr. rep. Y/OWI-8,* p. 130, Office of Waste Isolation, Oak Ridge Nat. Lab., Oak Ridge, Tenn., Nov. 1976.

Hood, M., Some results from a field investigation of thermo-mechanical loading of a rock mass when heater canisters are emplaced in the rock, presented at the *U.S. Symp. Rock Mech. 20th,* 1979.

Interagency Review Group on Nuclear Waste Management, Subground report on alternative technology strategies for the isolation of nuclear waste, *Rep. TID-28818,* Washington, D. C., Oct. 1978.

Iwai, K., Fundamental studies of fluid flow through a single fracture, Ph.D. thesis, Univ. of Calif., Berkeley, 1977.

Kappelmeyer, O., and R. Haenel, *Geothermics with Special Reference to Application,* Geopublication Associates, Berlin, Stuttgart, 1974.

Kisner, R. A., J. R. Marshall, D. W. Turner, and J. E. Vath, Nuclear waste projections and source-term data for FY 1977, *Rep. Y/OWI/TM-34,* Office of Waste Isolation, Oak Ridge Nat. Lab., Oak Ridge, Tenn., April 1978.

Lamb, H., *Hydrodynamics,* 6th ed., p. 583, Cambridge University Press, New York, 1932.

Martinez-Baez, L. F., and C. H. Amick, Thermal properties of Gable Mountain basalt cores, Hanford Nuclear Reservation, *Rep. LBL-7038,* Lawrence Berkeley Lab., Berkeley, Calif., 1978.

Meyer, C. A., R. B. McClintock, G. J. Silvestri, and R. C. Spencer, Jr., *1967 ASME Steam Tables,* American Society of Mechanical Engineers, New York, 1967.

National Research Council, The disposal of radioactive waste on land, report, Committee on Waste Disposal, Division of Earth Sciences, National Academy of Sciences, Washington, D. C., 1957.

Pratt, H. R., T. A. Schrauf, L. A. Bills, and W. A. Hustralid, Thermal and mechanical properties of granite, Stripa, Sweden, *Rep. TR-77-92,* Terra Tek, Salt Lake City, Utah, Oct. 1977.

Snow, D. T., A parallel-plate model of permeable fractured media, Ph.D. thesis, Univ. of Calif., Berkeley, 1965.

Witherspoon, P. A., J. S. Y. Wang, K. Iwai, and J. E. Gale, Validity of cubic law for fluid flow in a deformable rock fracture, *Water Resour. Res., 16*(6), 1016–1024, 1980.

Wooding, R. A., Steady free thermal convecting of liquid in a saturated permeable medium, *J. Fluid Mech., 2,* 273–285, 1957.

(Received June 28, 1979;
revised July 11, 1980;
accepted Dec. 16, 1980.)